EVALUATION OF STABILITY MARGIN INCLUDING NON-LINEAR CONTROL FOR AMB-EQUIPPED FLEXIBLE ROTOR

Kazuki Ikenaga, Osami Matsushita, Hiroyuki Fujiwara, Makoto Ito
National Defense Academy, Department of Mechanical Engineering
1-10-20 Hashirimizu, Yokosuka, Kanagawa, Japan, 239-8686
g42020@nda.ac.jp

ABSTRACT

Designing controllers is generally based on linear or non-linear control theory. An example of the former is the PID control that is the most popular and widely used in industries. An example of the latter is Variable Structure Control (VSC). In this study, we added the VSC to an AMB-equipped flexible rotor under the PID control. We used the sensitivity function, a way to potentially evaluate the stability margin of the AMB linear system by applying to the non-linear system of the VSC on the system stability. In order to study the VSC's stability effect quantitatively, we selected the following parameters: s and Δ of $k\Delta sign[(sx+\dot{x})x]x$, and the property of a front-stage filter.

1.INTRODUCTION

Recently, Active Magnetic Bearings (AMBs) featuring non-contact support is getting popular for industrial rotating machinery, and many studies for improving the performance are being conducted[1]. AMB controller design needs to sufficiently damp critical speeds appearing within the rated speed. Since a flexible rotor has lots of high-frequency eigen modes, it is easy to oscillate at the bending mode frequencies. Therefore, it is very important to suppress these modes for the system stability. Controller design is generally based on linear control theory. A typical example of the former is the PID control that is the most popular and widely used in industries. When a controller is designed according to the PID control, the phase lags of the plant and controller are taken into consideration to give some phase leads to the high frequencies[2]. Non-linear means for AMB control has been recently introduced. An example of the non-linear control is VSC including bang-bang and sliding mode control. The VSC changes control structure according to a switching rule specified arbitrarily. For such control, many reports have been provided[3,4]. The purpose of this paper is to exert non-linear control force having variable structure on an AMB-equipped flexible rotor being levitated by the PID linear control to check how much the non-linear force contributes to the stability through the sensitivity function.

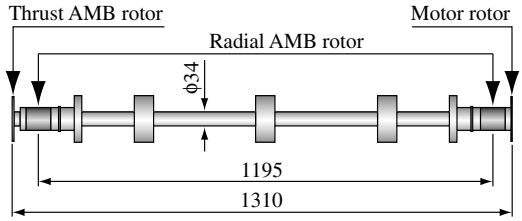

Figure 1: Structure of a flexible rotor

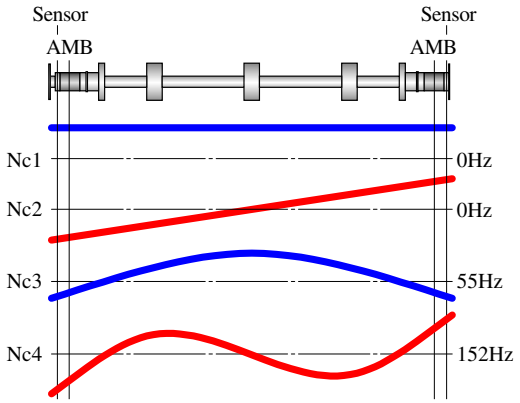

Figure 2: Mode shapes of the flexible rotor (free/free)

2. EXPERIMENTAL SYSTEM

2.1. Experimental system: Figure 1 roughly illustrates the flexible rotor we used. The shaft diameter is 34 mm, the length is 1,316 mm, and the mass is 31.4 kg. The rotor has three disks in the center and two disks at both ends so as to keep the balance during rotation. Moreover, thrust AMB and motor rotors are attached to the left and right ends respectively. Figure 2 shows the vibration modes of the flexible rotor from Nc1 to Nc4.

2.2. Description of the flexible rotor: Figure 3 is the critical speed map of the rotor. The vertical and horizontal axes show the natural frequency of the rotor and the stiffness of the AMB respectively, and the dashed line indicates the estimated stiffness of the PID control. Accordingly, the critical speeds are derived from the intersections of the solid (natural frequency) and dashed (AMB's stiffness) lines.

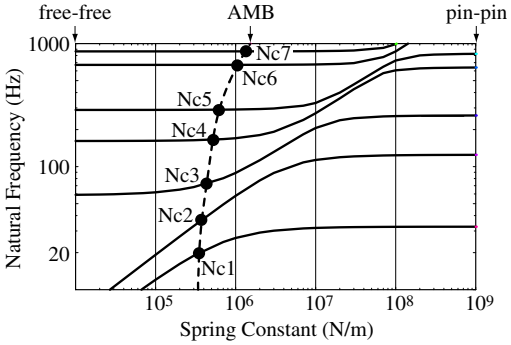

Figure 3: Critical speed map

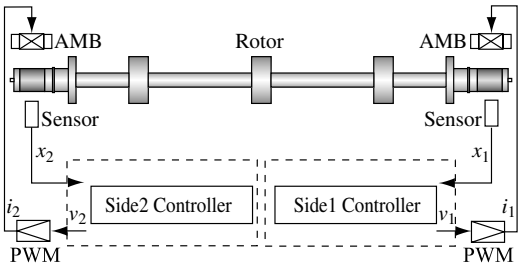

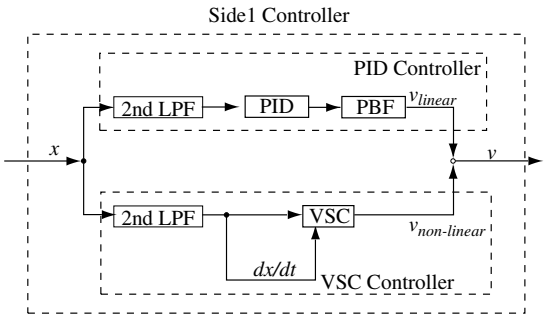

Figure 4: Block diagram of digital controllers

3. LINEAR CONTROLLER

3.1. Controller configuration: Figure 4 is a block diagram of the controllers we used. They are digital controllers using a Digital Signal Processor (DSP) and operating at a sampling frequency of 20 kHz. The control method is side-by-side control. The displacement of the AMB-equipped flexible rotor is measured by the sensors arranged close to each radial AMB. The main controller is designed according to the PID control and can levitate the rotor. The additional controller has variable structure, which will be described in the next section. Let us examine the effect of adding the VSC to the PID control through the sensitivity function. Note that the VSC is added only to Side 1 and that Side 2 is always controlled only by the PID control.

3.2. Digital controller configuration: Figure 5 is a block diagram of the digital controller. The sensor measures the AMB's displacement and feeds the resulting signal to the DSP via the sensor amplifier and low-pass filter (5 kHz). The DSP converts the displacement signal to the equivalent control force and then sends the corresponding value to the PWM amplifier (2A/V). The PWM amplifier lets the corresponding current flow through the coil to yield the AMB force.

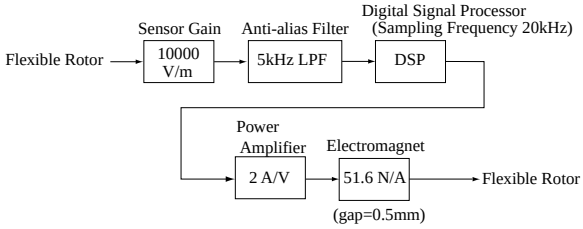

Figure 5: AMB system control block diagram

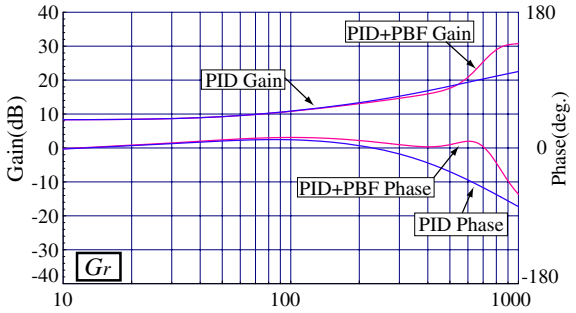

Figure 6: Bode plot of the PID controller's transfer function

3.3 PID controller configuration: Figure 6 is the Bode plot of the transfer function (G_r) of the PID controller. Since the measured phase lag of the plant is added to the phase plot, it represents the phase of the overall system. The controller uses not only the PID control but also a Phase Bump Filter (PBF) and a second-order Low-Pass Filter (2nd LPF). Figure 6 shows that compared to the use of only the PID control, the additional PBF further advances the phase at high frequencies, that is, it gives up to the seventh natural frequency (680 Hz) phase leads. The transfer function of the PID controller having the PBF is given by the following equation:

$$G_r = G_{PID}\ G_{PBF}\ G_{2ndLPF} \qquad (1)$$
$$where\ G_{PID} = G_I\ G_{PL1}\ G_{PL2}$$

G_I, G_{PL}, G_{2ndLPF}, and G_{PBF} are the transfer functions of the integration circuit, phase lead circuit, 2nd LPF, and PBF respectively, and each is represented as follows:

$$G_I = \frac{1}{\tau_1 s} \quad G_{PL1} = \frac{\tau_2 s + 1}{\alpha_1 \tau_2 s + 1} \quad G_{PL2} = \frac{\tau_3 s + 1}{\alpha_2 \tau_3 s + 1}$$

$$G_{2ndLPF} = \frac{1}{(\tau_5 s)^2 + 2\zeta_2(\tau_5 s) + 1}$$

$$where\ \tau_1 = \frac{1}{2\pi 0.1}; \tau_2 = \frac{1}{2\pi 50}; \tau_3 = \frac{1}{2\pi 140}; \tau_4 = \frac{1}{2\pi 800};$$

$$\tau_5 = \frac{1}{2\pi 5000}; \alpha_1 = 0.4; \alpha_2 = 0.1; \zeta_1 = 0.25; \zeta_2 = 0.2$$

3.4. Static levitation test with the PID control:

Figure 7 is a block diagram of the closed-loop control system we used. During levitation, signals are measured at the input/output points from ① to ④. A excitation signal is supplied to ①, and the resulting signals are measured at ③ and ②. Namely, the plant transfer function G_p is represented as ③/②. Moreover, measuring the

resulting signal at ④ gives the open-loop transfer function G_o = ④/②. The PID controller mentioned before statically levitates the AMB-equipped flexible rotor. Figures 8 and 9 show the measured G_p and G_o respectively, and the former clearly indicates the peaks of each mode. Figure 10 is the Nyquist plot of G_o. Since the Nyquist plots of Nc4 and Nc5 are sufficiently apart from the critical point (-1,0), this shows that both modes are stable.

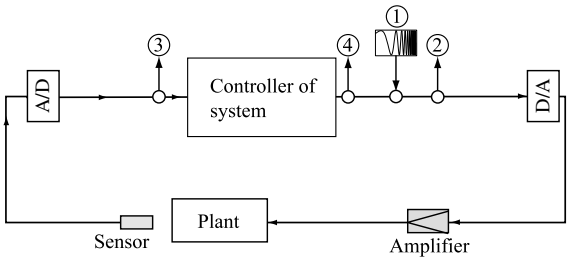

Figure 7: Block diagram of the AMB system

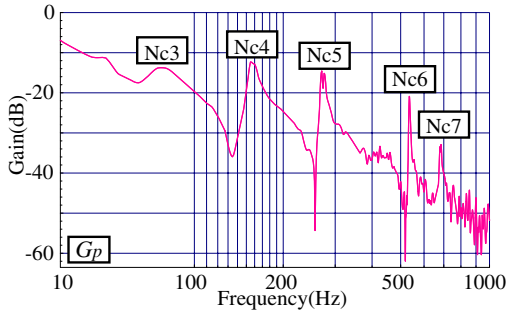

Figure 8: Bode plot of the plant transfer function

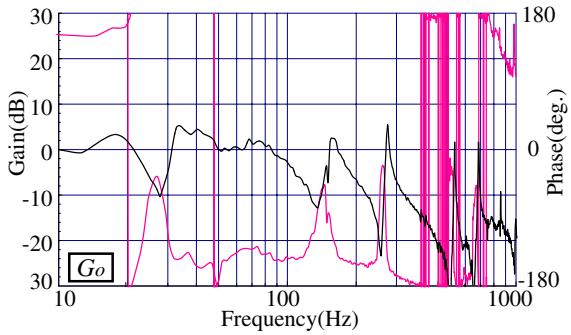

Figure 9: Bode plot of the open-loop transfer function

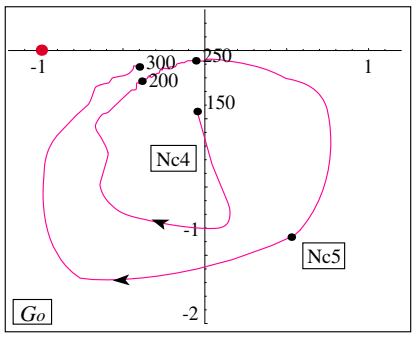

Figure 10: Nyquist plot of the PID system (150-300 Hz)

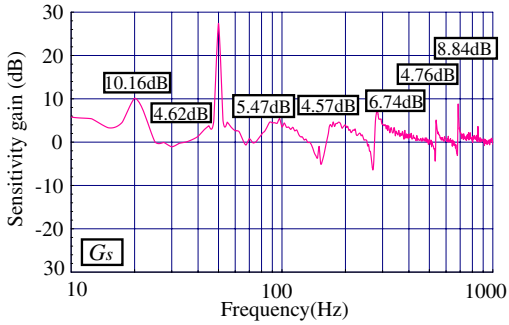

Figure 11: Sensitivity function of the PID system

3.5. Sensitivity function measurement:

The sensitivity function[5] is given by the following equation:

$$G_s = \frac{1}{1+G_o} \qquad (2)$$

The sensitivity function G_s is the reciprocal of the distance from the critical point (-1,0) to G_o. Therefore, the shorter the distance, the greater the G_s value, and the longer the distance, the smaller the G_s value. This means that if the rotor stably levitates a little, the open-loop transfer function G_o and the sensitivity function G_s can be measured to evaluate the stability margin through the resulting sensitivity function. G_s is represented as ②/① in Figure 7. Figure 11 shows the resulting G_s during static levitation with the PID control. The peak at 50 Hz is ignored because it is caused by power source noise. The figure also presents the sensitivities of each mode from Nc1 to Nc7.

4. ADDITIONAL VSC

4.1. VSC design: The VSC controller we employed is given by the following equation:

$$\Psi = k\Delta sign[\sigma x]x \qquad (3)$$

$$where\ \sigma = s x + \dot{x}\ \ (\Delta < 1)$$

Here, σ is a switching line changing the control force. Since the sign of the control force is changed at σ =0 and x=0, the VSC's property changes four times in the overall system. Figure 12 shows these changes on the phase plane. Since the structure of equation (3) changes according to the parameter s, it is possible to arbitrarily specify an area where positive and negative springs are added. The parameter k is a constant providing the AMB's stiffness when the rotor is levitated by the PID control, while the parameter Δ is a variable determining the VSC's stiffness against the PID control. In general, the velocity amplitude A' detected along with the vibration amplitude A is represented as $A'=\omega A$ where ω is the frequency. Accordingly, high-frequency speed is dominant in multiple-mode vibration. In this study, using the 2nd LPF for the input signal to the VSC eliminates the effect of the high frequencies as shown in Figure 4, and the effect of a specific mode frequency is examined. Figure 13 shows the characteristics of the 2nd LPF we used.

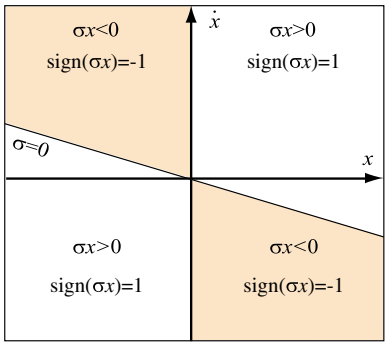

Figure 12: Phase portraits for the VSC model

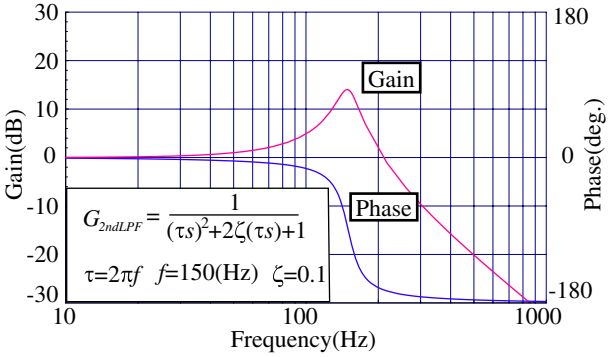

Figure 13: Transfer function of the 2nd LPF

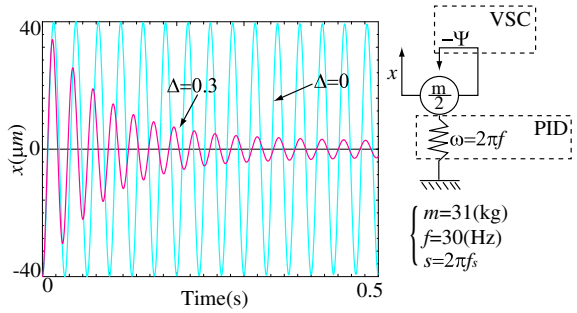

Figure 14: Simulation of an 1DOF model

4.2. VSC damping effect: Figure 14 illustrates a 1DOF system when equation (3) is introduced theoretically. The system has half the rotor mass and a stiffness corresponding to a natural frequency of 30 Hz. In equation (3), Δ is 0.3 and a control force of about 30 percent of the AMB's stiffness is exerted. The figure also indicates the resulting step response, which shows that equation (3) can damp the system effectively.

5. EVALUATING THE STABILITY MARGIN WITH NON-LINEAR CONTROL

5.1. Evaluation criteria of ISO: Subsection 3.6 described how to measure the sensitivity function while ISO CD 14839-3 defines the criteria for evaluating the stability margin of a system having an AMB-equipped flexible rotor through the sensitivity function. Table 1 lists the allowable sensitivities specified by ISO. Of all eigen modes, the mode having the highest sensitivity is found, and its zone provides the stability margin of the overall system. According to ISO CD 14839-3, the PID control system shown in Figure 11 has a maximum sensitivity of 10.16 dB at Nc1, so it is classified into Zone B.

Table 1: Peak sensitivity at zone limits

Zone	Peak sensitivity	
	level	factor
A/B	8dB	2.5
B/C	12dB	4
C/D	14dB	5

5.2. Stability margin evaluation test: Equation (3) has three parameters: the gain ratio Δ of the PID control, the coefficient s of the switching line, and the corner frequency f_{2nd} of the 2nd LPF. In this test, we examined how the sensitivity function was changed when $\Delta = 0.3$ and the switching line coefficient and corner frequency varied.

5.2.1. Effect of the switching line coefficient: We used three variable structure controllers having different slopes to measure the sensitivity functions. Figure 15 shows the resulting sensitivity functions. Letting the corner frequency of the 2nd LPF (Figure 13) be 150 Hz and the coefficient of the switching line be $s=2\pi f_s$ (rad/s), the effect of f_s is examined. The figure shows that as f_s shifts from 100 Hz to 200 Hz, the 200 Hz sensitivity reduces and is finally lower than the sensitivity given by the PID control. As shown in Figure 13, the 2nd LPF has a high gain near the corner frequency. These results mean that the VSC is affected by the coefficient of the switching line and the corner frequency.

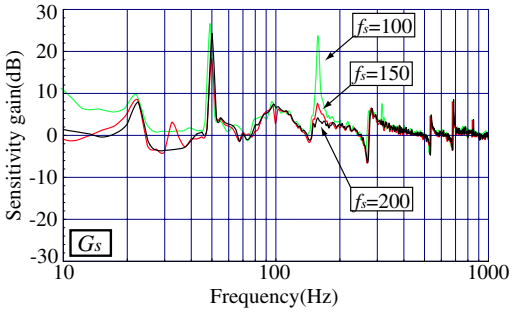

Figure 15: Sensitivity function of the system (PID + VSC)

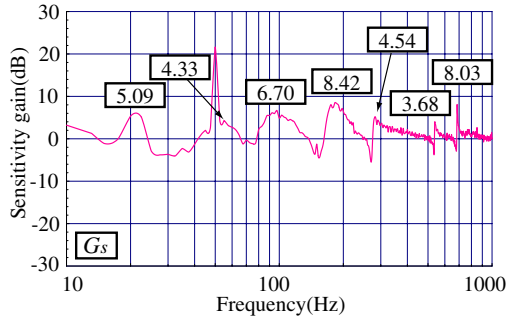

Figure 16: Sensitivity function of the system (Case 2)

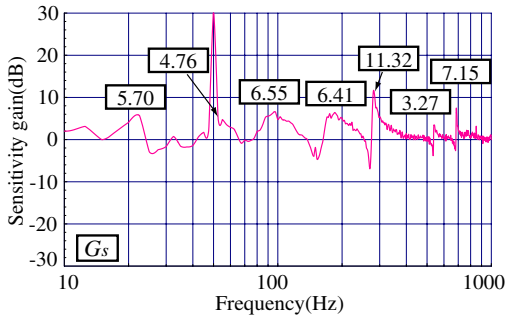

Figure 17: Sensitivity function of the system (Case 3)

Table 2: Specifications of the controller

	f_{2nd} (corner frequency of the 2nd LPF)	f_s (switching frequency)
Case 1	150 Hz	300 Hz
Case 2	230 Hz	460 Hz
Case 3	400 Hz	800 Hz
Case 4	500 Hz	1000 Hz
Case 5	610 Hz	1220 Hz
Case 6	640 Hz	1280 Hz

Table 3: Differences from the PID peak sensitivities in each case

	Nc1	Nc2	Nc3	Nc4	Nc5	Nc6	Nc7
PID	10.16	4.62	5.47	4.57	6.74	4.76	8.84
Case1	-4.57	-	1.91	-1.41	-	-	-1.28
Case2	-5.07	-	1.23	3.85	-2.2	-1.08	-
Case3	-4.46	-	1.08	1.84	4.58	-1.49	-1.69
Case4	-4.19	-	-	1.59	3.77	-2.47	-2.05
Case5	-3.21	1.14	-1.21	-	2.27	-	-2.78
Case6	-4.11	-	-	1.48	2.96	-	-2.28

5.2.2. Effect of corner frequency of the 2nd LPF:

Based on the results mentioned in the previous subsection, the frequency f_s of the switching line coefficient was set twice as high as f_{2nd} to ensure that the VSC was effective. We then measured the sensitivity function when f_{2nd} varied. Table 2 shows the parameter values of the VSC. Figures 16 and 17 show the resulting sensitivity functions of Cases 2 and 3 respectively. Both indicate that the sensitivity decreases at the frequency nearest to and higher than f_{2nd} and increases at lower frequencies. Table 3 lists the sensitivity differences between this test and the PID control shown in Subsection 3.6. As a difference of ±1 dB falls within the range of possible error, it is shown by a minus "–" symbol in the table. The table shows that Nc1 becomes lower in all cases and that almost all sensitivities decrease at frequencies higher than f_{2nd} and increase at frequencies lower than f_{2nd}. Based on these results, we conducted the same test with other parameters, but we found no parameter that was able to reduce the sensitivities over all frequencies.

6.ROTATION TEST

Figure 18 shows the rotation test results. In both cases of the PID control and of PID + VSC, the rotor was able to turn at up to 70 rps via the second rigid mode. The vibration amplitude of PID + VSC was smaller than that of only the PID control. We will add balancing technologies to overcome the bending critical speed in the future.

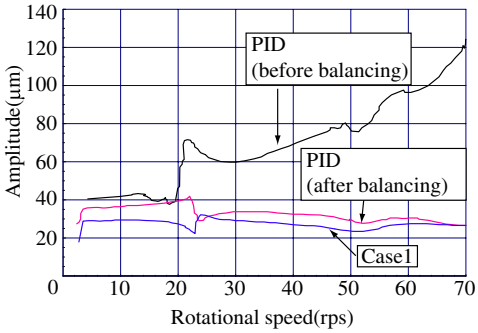

Figure 18.Resonance plot for each case

7. CONCLUSIONS

In this study, we added the VSC to the AMB equipped flexible rotor under the normal PID control. We employed the combination of the VSC and 2nd LPF to check how the corner frequency of the filter and the switching line coefficient of the VSC affect the stability margin through the sensitivity function. The results are described below.

1. The VSC is very effective around the corner frequency if the 2nd LPF is used together.
2. The coefficient of the switching line σ greatly varies around each natural frequency, and our test shows that the greater the slope, the better the result.
3. The sensitivities of the rigid modes and the modes higher than the corner frequency of the 2nd LPF decrease, but the sensitivities of the modes nearest to and lower than the corner frequency increase.

REFERENCES

[1]G.Schweitzer, Active magnetic bearing - chance and limitations, Proc. 6th Int. Conf. on Rotor Dynamics (IFToMM-6), pp.1-14, 2002

[2]Kouji Ebina, et. al., Robustness and Stability Margin of a Flexible Rotor Supported by Active Magnetic Bearing, Proc. 6th Int. Sym. on Magnetic Suspension Technology, Turin Italy, pp.70-75, 2001

[3]Takuzo Iwatubo, et. al., Modified Bang-Bang Control for Vibrations of Active Magnetic Bearing Equipped Rotor, Trans. of JSME, vol64-627, pp.100-106, 1998 (In Japanese)

[4]John Y.Hung, Variable Structure Control: A Survey, IEEE Trans. Ind. Election, vol40-1, pp.2-22, 1993

[5]Hiroyuki Hujiwara, et. al., Control of Flexible Rotors Supported by Active Magnetic Bearings, Proc. 8th Int. Symp. on Magnetic Bearing, pp.145-150, 2002.